Chapter 6

PHOTONIC DEVICE CHARACTERIZATION

Experimental setup

A home-built optical confocal microscope setup is used to characterize the fabricated ring resonators. The diagram of the setup is shown in figure 6.1 and the pictures of the actual setup are in figure 6.2. A 950 nm long-pass dichroic mirror was used to filter 780 nm excitation laser for spectroscopy measurements. For ODMR measurements, the nitrogen gas transfer port was replaced by SMA ports that can be connected to MW sources. Each ZPL of divacancies (PL1-4) was filtered using tunable longpass and shortpass filters. A superconducting nanowire single photon detector (SNSPD) was used for lifetime measurements on divacancies and Cr ions. An InGaAs detector after a beam splitter was used for the timing input to the time correlated photon counting board. A supercontinuum laser with repetition rate of 20 MHz and 2 kHz was used for divacancies (lifetime ~15 ns) and Cr ions (lifetime ~130 μs) accordingly. The coarse resonance measurements of Si ring resonators were performed using a near IR spectrometer with a supercontinuum source. The gratings in the spectrometer are able to measure quality factors up to ~30,000 reasonably. The nitrogen gas tuning can typically tune resonances of silicon ring resonators for ~1.5 nm at 1070 nm.

To further characterize the resonance in higher resolution, I built a tunable external cavity diode laser with Littman-Metcalf configuration using Thorlabs kit (TLK-L1050M) with AR coated diode (LD-1050-0050-AR-2) purchased from Toptica as shown in figure 6.3. The coherent light was generated by stimulated emission with the help of an external cavity between the end face of the diode and the mirror. The feedback light that selects the wavelength of amplified light comes from the 1st order diffraction from the grating, and it was reflected back by a mirror in Littman configuration. The direction of the output laser is fixed during tuning because the output is the reflected light (0th order diffraction) from the grating, which is a main advantage over Littrow configuration. The wavelength tuning can be performed by moving the angle of the mirror and by sending back light with a different wavelength. The mirror can be controlled either with a DC servo motor (Z812) or with a piezoelectric actuator attached to the contact point of the motor and the mirror arm. The maximum power is 50 mW around 1040 nm and > 10 mW in the range 1020-1085 nm before fiber coupling.

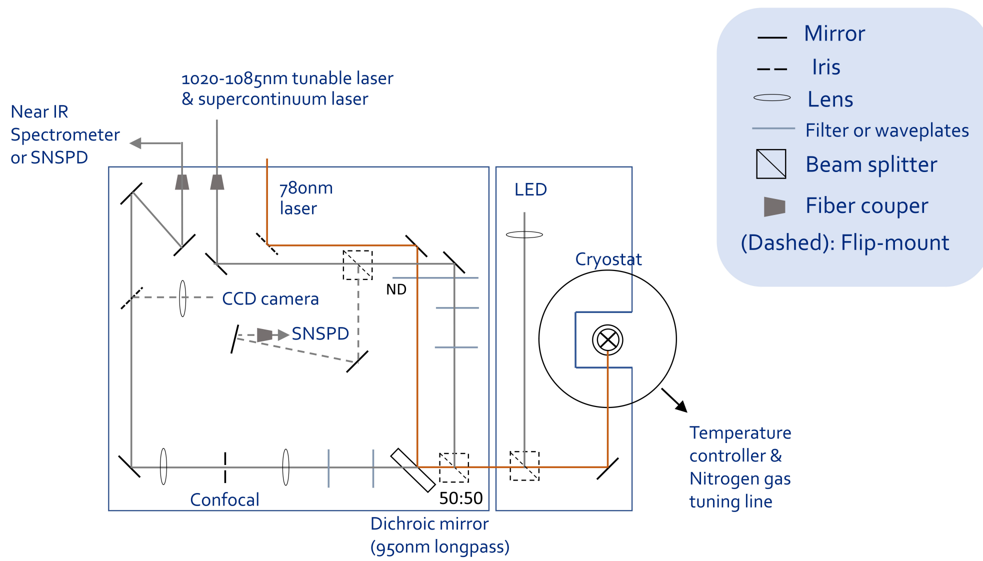

Figure 6.1: The optical confocal microscope setup diagram.

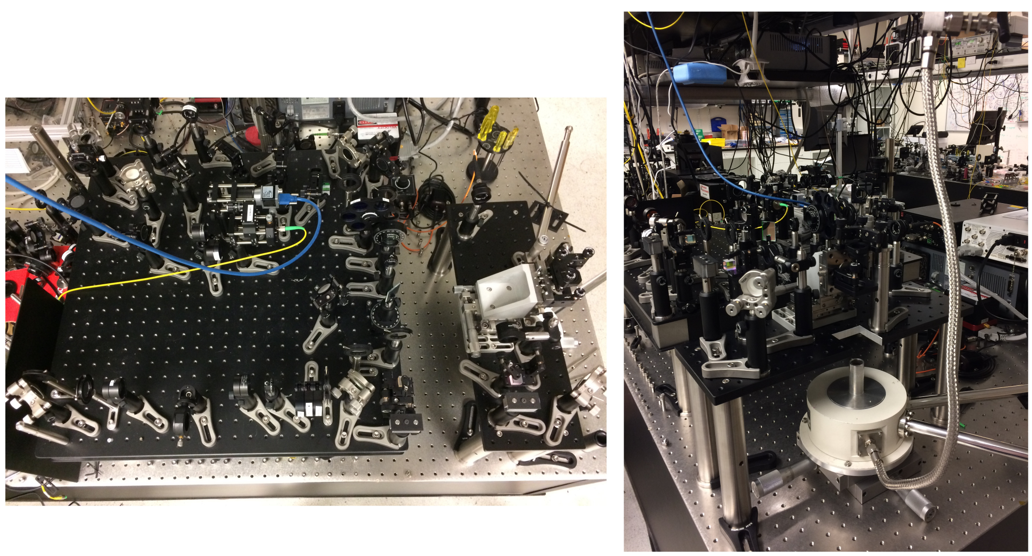

Figure 6.2: The actual setup (left) viewed from top and (right) viewed from the right.

Mode hop free tuning for a relatively large frequency range was required for scanning a resonant peak of an optical resonator. The mode hops occur when the next mode

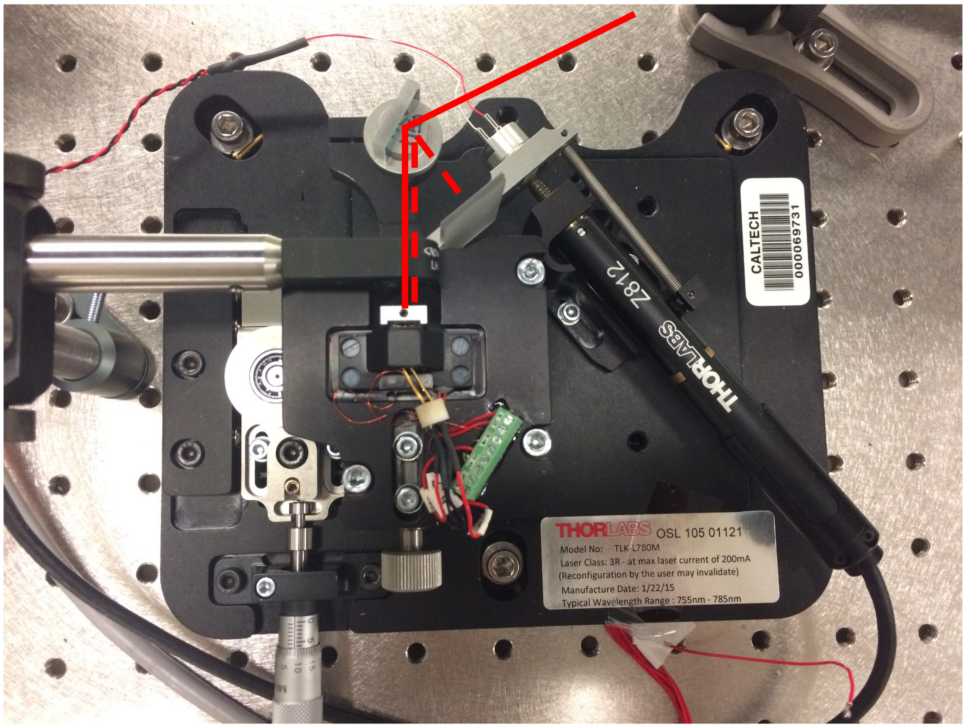

Figure 6.3: The actual Littman configuration in the setup. The red solid lines show the main laser path and the dotted line shows the feedback path.

has more optical feedback than the current mode, which often happens when the resonant peak of internal cavity formed by two end diode faces and of the external cavity don't match. We need to maintain both cavity gain peaks aligned during wavelength tuning. The internal cavity resonance moves by changing the diode current. The current and piezoelectric actuator voltage need to be changed at the same time with an optimized ratio to prevent mode hops[91]. The wavelength change of the internal cavity mode peak against diode current is expressed by $\beta = \frac{\Delta\lambda}{\Delta I_{LD}}$. To measure β, the laser diode output without feedback was measured using an optical spectrum analyzer for different diode current. Part of the measurements for low current 40-60 mA are shown in figure 6.4. β=2.2 GHz/mA at low current and β=2.6 GHz/mA at high current around 150 mA.

After lasing was confirmed with alignment, laser modes are monitored using a scanning fabry-perot interferometer. When the feedback is not optimal the laser operates in multimode with next mode separated by 1.9 GHz corresponding to ~8 cm external cavity length. After single mode operation is confirmed at fixed wavelength, the output power is maximized by optimizing the alignment. Then

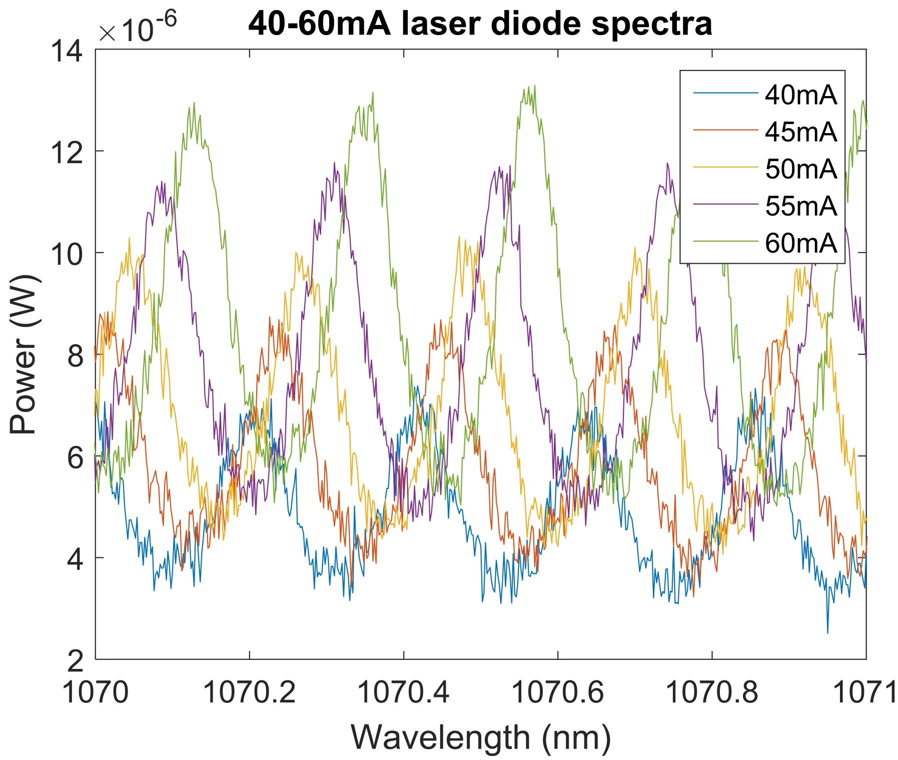

Figure 6.4: The internal cavity resonances change due to different diode current (40-60 mA).

piezo tuning as a function of applied voltage $\frac{\Delta\lambda}{\Delta V_{PZT}}$ was measured with a fixed fabry-perot resonance. With previously measured β, I built an inverting amplifier that controls the laser diode current depending on the piezoelectric actuator voltage so that internal and external cavity modes move at the same rate. I used a potentiometer for one of the 2 resistors to adjust the change of β at higher diode current during tuning. The external signal proportional to the piezo voltage is input to the inverting amplifier and its output was fed to the laser current controller.

After single mode operation in a full piezo scan without mode hops was confirmed, piezo calibration was performed. Piezo movements are not linear against applied voltage and the wavelength change per unit voltage change at different piezo voltages was measured as shown in figure 6.5. Piezo modulation of 1 Hz triangular wave (0-150 V) is used for measurements. The InGaAs detector of the IR spectrometer continuously takes frames during the scanning and the photon counts at every wavelength pixel is integrated for each frame as output signal. Because the linewidth of laser was not measured and it is less than the 67 MHz scanning fabry-perot resonance FWHM, the scanning frequency is adjusted so that this scanning method can give 95 MHz resolution. 1 GHz separated sidebands were added by electro-optic modulator as a standard and changed the resonance of a scanning fabry-perot to measure peak to peak separation in the range of 0-150 V. The resulting curve was fitted and used for correction of resonance scan data.

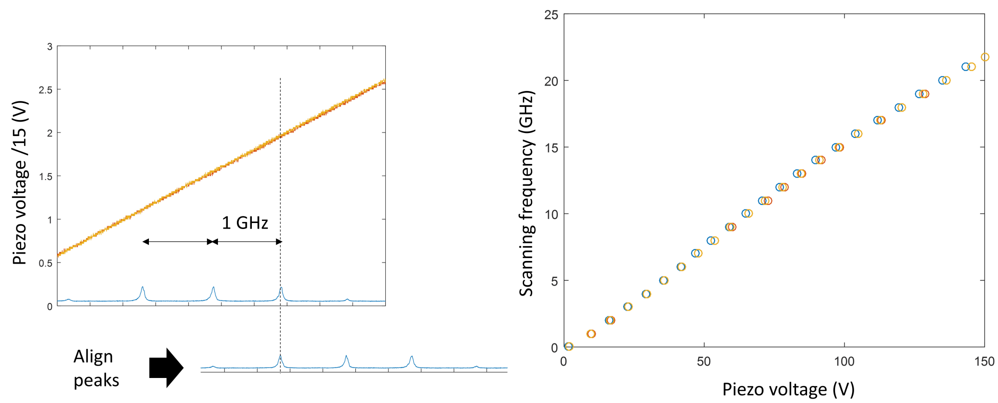

Figure 6.5: The actual Littman configuration in the setup. The red solid lines show the main laser path and the dotted line shows the feedback path.

The laser power is modulated during scanning and the laser power versus diode current was measured to provide correction to scan data as well. The laser power is almost linear to the diode current as shown in the left panel of figure 6.6. The stability of the laser power was measured over 8 hours to verify that the laser is stable enough for scanning measurements as long as a couple seconds each, as shown in the right panel of figure 6.6. The wavelength shift was < 1.0 pm/hr.

c-Si on SiC resonators measurement results

The measurements of the quality factor of ring resonators were mostly performed by focusing the laser on the input port and collecting the output from the drop port as shown in figure 6.7. One of the best ring resonators has a quality factor of 23000 at 1078 nm measured at 20 K. The measurement results are shown in figure 6.8. The condition for critical coupling of ring resonators coupled with two waveguides is $\alpha = \frac{t_1}{t_2}$, where α is ring round-trip loss coefficient, t_1 is the self coupling coefficient

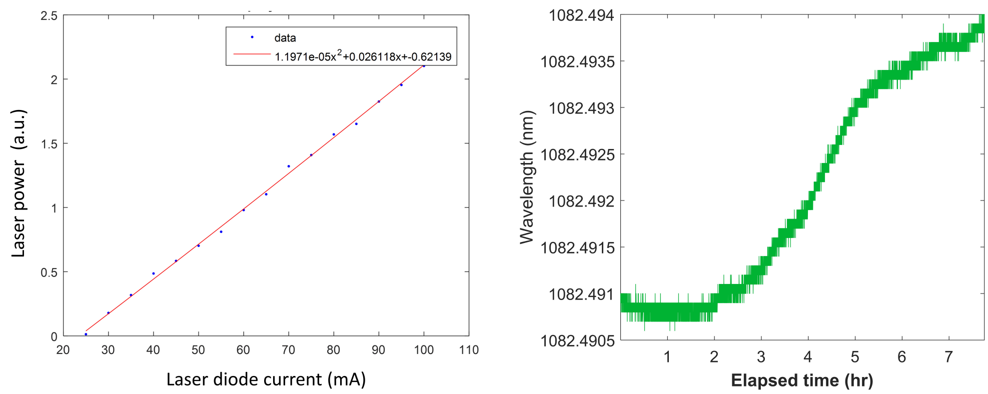

Figure 6.6: The ECDL power drift over 8 hours.

from input to throughput port and t_2 is self coupling coefficient from add to drop port. Because there is always loss ($\alpha \neq 1$), the symmetrical waveguide design that we used is never at critical coupling condition.

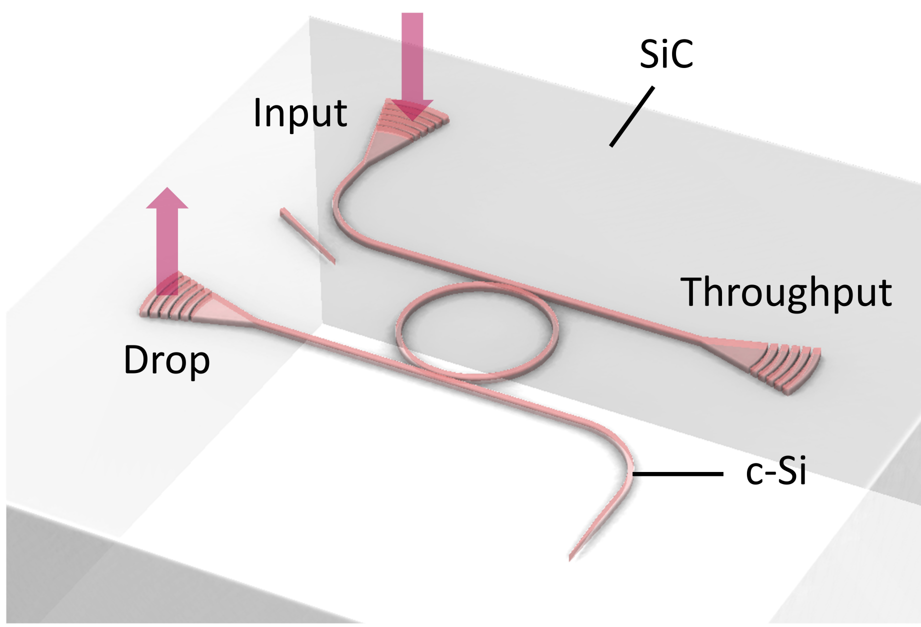

Figure 6.7: Main measurements were performed through the drop port.

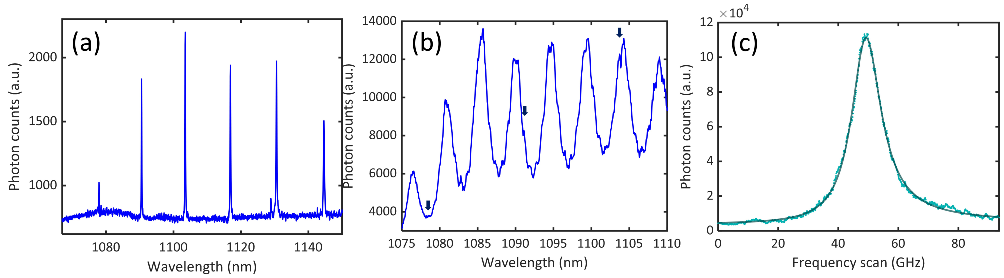

Figure 6.8: (a)Coarse measurement through the drop port with supercontinuum laser. (b)Coarse measurement through the thoroughput port. Arrows indicate the locations of resonances. (c) Fine measurement with tunable laser scanning. The Lorentzian fit reveals Q~23000.

The Purcell factor for a qubit in hybrid cavities is[36]:

$$F_{ZPL} = \frac{3}{4\pi^2}\left(\frac{\lambda_{ZPL}}{n_c}\right)^3 \frac{n_c}{n_h}\frac{Q}{V}\left|\frac{\boldsymbol{E}(\boldsymbol{r}_{qubit})}{\boldsymbol{E}(\boldsymbol{r}_{max})}\right|^2 \tag{6.1}$$

Based on simulation and measurements, the mode volume of the ring resonator is 19.5 and the best measured quality factor is 23000 at a wavelength of 1078 nm. This would result in a Purcell enhancement factor of 36 assuming perfect dipole alignment for an emitter located at 10 nm below the surface. The estimated Purcell enhancement factor for an emitter at a depth of 100 nm is 12 due to a 3 times smaller field.

6.1 Conclusion

We were able to fabricate on-chip silicon ring resonator on 4H-SiC with quality factor of 23000. The crystalline silicon membrane transfer method described in 5.4 can be used to successfully place membranes as a photonic device layer on silicon carbide and potentially other host materials. The smooth surface of crystalline silicon has the potential to achieve better quality factor than amorphous silicon devices. The change from a-Si to c-Si or using resist reflow technique only improved the quality factor by order of 2. This suggests the limiting factor is surface or material absorption of silicon used in this work.

Chapter 7

CONCLUDING REMARKS

In my Ph.D. projects, I fabricated Si on SiC hybrid ring resonators to couple ZPL emissions of divacancies in 4H-SiC. Photonic devices such as ring resonators can be used to enhance coherent emission for indistinguishable photons used in quantum networks. Quantum entanglement generation rate is a key measure for the distance at which quantum communication can be established. This rate scales linearly or with higher order with indistinguishable photon generation rate, which makes enhancing coherent emission of qubits an important engineering challenge.

Among different qubits, divacancy defects in 4H-SiC recently emerged as promising candidates with long spin coherence time and good optical stability compared to NV centers in diamond (See chapter 2). I alsoe studied a few other impurities like Cr and Mo ions in 4H-SiC and they were found to possess relatively short T_2< 1 μs, which does not satisfy the high fidelity qubit polarization condition. My research is mainly focused on divacancies in 4H-SiC and fabrication of photonic devices on 4H-SiC. The ZPL emission of divacancies is useful as indistinguishable photons for entanglement generation, which only consists of ~5% of total emission. In order to unleash the potential of divacancies it is important to enhance only the usable coherent emission with narrow-linewidth photonic devices. In my research I developed a fabrication method for silicon ring resonators on SiC (or on other materials). Silicon is used for the photonic device layer. This hybrid approach avoids charge build-up around the qubits, which is believed to degrade optical properties of the emitters. It is transparent and suitable for coupling divacancy's near IR wavelength from 1050 nm as shown in chapter 4.

4H-SiC is widely used for power electronics devices and readily available in mass production. Recently, a single divacancy residing in commercially available p-i-n diodes showed T_2 ~1 ms at 5K [92]. Integrating qubit host materials with classical semiconductor devices might be beneficial as a new type of quantum devices. The Si photonic devices shown in this thesis are compatible with this platform as long as divacancies are located in the proximity to the surface. Silicon integrated photonics is currently accepted as a next generation power-efficient classical telecommunication platform [93]. The advantage is low-cost and high-volume silicon photonic on-chip devices manufacturing that is compatible to the CMOS technology. The Si hybrid devices can be readily integrated with a variety of Si components such as filters, multiplexers, modulators and sensors. Additionally, integration between silicon photonics and superconducting nanowire single photon detectors (SNSPDs) [94] can enable on-chip spin-spin entanglement platform and a range of quantum technologies.

For quantum emitters with lower than 1050 nm wavelength, different material is required for the optical device layer. For example, silicon vacancies (V_{Si})in 4H-SiC exhibits ZPL at 860 and at 920 nm [95]. Materials such as GaAs with bandgap 1.44 eV (300 K) is transparent enough for silicon vacancies at low temperature. Currently, our group is developing GaAs hybrid photonic devices for Yb^3+ ions in YVO with optical transition at 984 nm [96]. GaP with bandgap 2.24 eV (300 K) can be used for confining light with shorter wavelength > 600 nm including ZPL of NV centers in diamond at 637 nm [97].

Direct device fabrication on SiC membranes can achieve largest light confinement at the the spot of qubits in SiC, achieving strong enhancement of the emission. Vuckovic group showed 4H-SiC photonic crystal on insulator with fusion bonding technique [98]. If this can be expanded to wafer scale bonding, mass production of on-chip quantum networks will be possible.